

## **Evaluation of Interconnection Configuration Schemes for PV Modules with Switched-Inductor Converters under Partial Shading Conditions**

Niazi, Kamran Ali Khan; Yang, Yongheng; Nasir, Mashood; Séra, Dezso

*Published in:*  
Energies

*DOI (link to publication from Publisher):*  
[10.3390/en12142802](https://doi.org/10.3390/en12142802)

*Creative Commons License*  
CC BY 4.0

*Publication date:*  
2019

*Document Version*  
Publisher's PDF, also known as Version of record

[Link to publication from Aalborg University](#)

### *Citation for published version (APA):*

Niazi, K. A. K., Yang, Y., Nasir, M., & Séra, D. (2019). Evaluation of Interconnection Configuration Schemes for PV Modules with Switched-Inductor Converters under Partial Shading Conditions. *Energies*, 12(14), 1-12. Article 2802. <https://doi.org/10.3390/en12142802>

### **General rights**

Copyright and moral rights for the publications made accessible in the public portal are retained by the authors and/or other copyright owners and it is a condition of accessing publications that users recognise and abide by the legal requirements associated with these rights.

- Users may download and print one copy of any publication from the public portal for the purpose of private study or research.
- You may not further distribute the material or use it for any profit-making activity or commercial gain
- You may freely distribute the URL identifying the publication in the public portal -





### **Take down policy**

If you believe that this document breaches copyright please contact us at [vbn@aub.aau.dk](mailto:vbn@aub.aau.dk) providing details, and we will remove access to the work immediately and investigate your claim.



## Article

# Evaluation of Interconnection Configuration Schemes for PV Modules with Switched-Inductor Converters under Partial Shading Conditions

Kamran Ali Khan Niazi <sup>1,\*</sup> , Yongheng Yang <sup>1</sup> , Mashood Nasir <sup>2</sup>  and Dezso Sera <sup>1</sup> <sup>1</sup> Department of Energy Technology, Aalborg University, 9220 Aalborg, Denmark<sup>2</sup> Electrical Engineering Department, Lahore University of Management Sciences, Lahore 54792, Pakistan

\* Correspondence: kkn@et.aau.dk

Received: 6 June 2019; Accepted: 19 July 2019; Published: 21 July 2019



**Abstract:** Partial shading on photovoltaic (PV) arrays reduces the overall output power and causes multiple maximas on the output power characteristics. Due to the introduction of multiple maximas, mismatch power losses become apparent among multiple PV modules. These mismatch power losses are not only a function of shading characteristics, but also depend on the placement and interconnection patterns of the shaded modules within the array. This research work is aimed to assess the performance of  $4 \times 4$  PV array under different shading conditions. The desired objective is to attain the maximum output power from PV modules at different possible shading patterns by using power electronic-based differential power processing (DPP) techniques. Various PV array interconnection configurations, including the series-parallel (SP), total-cross-tied (TCT), bridge-linked (BL), and center-cross-tied (CCT) are considered under the designed shading patterns. A comparative performance analysis is carried out by analyzing the output power from the DPP-based architecture and the traditional Schottky diode-based architecture. Simulation results show the gain in the output power by using the DPP-based architecture in comparison to the traditional bypassing diode method.

**Keywords:** partial shading; photovoltaic (PV) arrays; multiple maximas; mismatch; differential power processing (DPP); series-parallel (SP); total-cross-tied (TCT); bridge-linked (BL); center-cross-tied (CCT)

## 1. Introduction

Solar energy is free and abundant [1]. Environmental concerns are widely reduced by using solar energy for power generation. Therefore, the photovoltaic (PV) energy is becoming the most emerging and promising solution to address environmental problems. Generally, the efficiency of solar PV energy conversion using PV panels is low [2], and therefore, many researchers are working on improving the efficiency and output energy yield [3]. Factors that may affect the conversion efficiency generally include the effect of soiling, dirt and dust, elevated temperature, and sudden irradiance changes [4]. Similarly, the output power produced by PV arrays is remarkably reduced due to partial shading conditions [5,6]. Partial shading is generally induced over a PV module, string, or on a whole small PV system. It is due to cloud shadows, dust, permanent cracks on shields or surfaces; as well as shade due to various structures including trees, leaves, and buildings or towers [7]. Partial shading causes a reduction in the irradiance, and also distributes irradiance in a non-uniform pattern over the surface of various PV modules in an array [8,9]. Hence, the current from the PV array is constrained by the shaded PV modules, which in turn is detrimental for the other healthy PV modules connected in the series [10]. Consequently, in practice, a parallel-connected diode termed as a bypass diode ( $D_1$  and  $D_2$ ) is installed across it to minimize the effects of mismatching, as shown in Figure 1a. During mismatching, this bypass diode will be ON and the current starts flowing through it (as shown in

Figure 1b). In this case, various maximas appear on the power–voltage (P–V) characteristics. These multiple peaks are known as local maxima's, as exemplified in Figure 1c. When multiple peaks are present, the conventional maximum power point techniques (MPPTs) may not work accurately. Therefore, a global maximum power point technique (GMPTT), capable to distinguish between local and global maxima is generally needed to maximize the overall output power from the array. In the literature, many conventional MPPT techniques have been presented and their behavior on partial shading conditions is analyzed [11–13]. Various artificial intelligence techniques including fuzzy logic [14,15], neural networks [16], and genetic algorithms [17] are generally employed to track the global maximum power point (GMPP). However, these techniques have limitations and exhibit false tracking over varying conditions of irradiance and temperature. Furthermore, the conventional MPPT methods should be retrofitted with more sensing and control requirements [18,19].

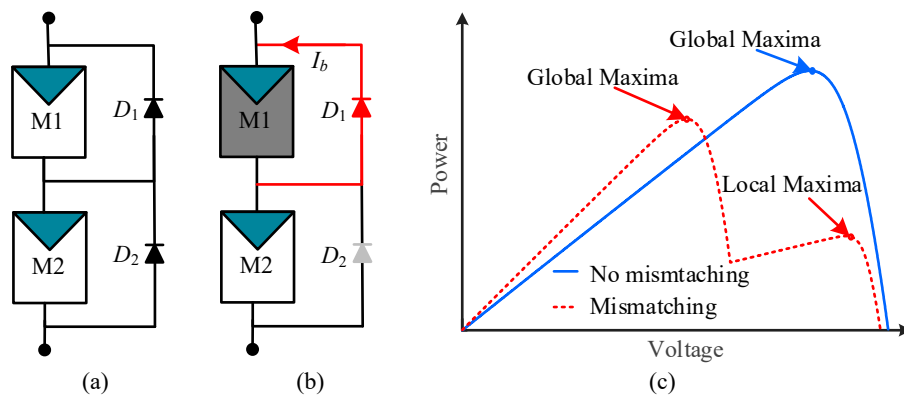


**Figure 1.** A PV module (M1 and M2) with parallel-connected bypass diodes  $D_1$  and  $D_2$ : (a) schematic diagram, (b) schematic showing the current flow direction while shaded and bypassed [19], (c) P–V characteristic of series-connected two PV modules while one is shaded (mismatching occurs). Here,  $I_b$  is a bypass current through  $D_1$ .

In addition to developing advanced MPPT algorithms, an alternative is to directly mitigate the local peaks under partial shading. Differential power processing (DPP) converters [20–25] are typical representatives, that enable each PV module to produce maximum output power. DPP converters eliminate the problem of multiple maximas in the PV string, as highlighted in Figure 2. In addition, Figure 3a further exemplifies one DPP configuration known as the PV–PV voltage balance converter [20]. This PV–PV converter only processes the mismatched power and thus, it is used in this paper. The working principle of the PV–PV DPP is shown in Figure 3b,c, where the PV module M1 is shaded and the PV module M2 in the non-shaded mode.  $I_L$  is a mismatch current, which passes through the inductor  $L$ . The transistors  $Q_1$  and  $Q_2$  operate complementarily to each other. Nevertheless, the switching will induce power losses that can be found as [20]

$$P_{SWLOSS} = 2k_0 \left[ V_G \sqrt{\frac{V_G}{2V_B}} + 4V_D I_L \sqrt{\frac{V_D}{V_B}} \right] f_{sw} \quad (1)$$

in which  $k_0$  is a material property dependant device constant,  $V_B$  is the breakdown voltage of the device,  $V_D$  is the voltage at the device terminal,  $V_G$  is the voltage at the gate terminal,  $I_L$  is the current passing through the inductor, and  $f_{sw}$  is the switching frequency of the power device. The PV–PV DPP topology is based on the switched-inductor between two PV modules. Therefore, it is named as switched-inductor (SL)-based topology. The SL-based topology can be represented by a simplified model as illustrated in Figure 4. To have the same voltage (i.e.,  $V_1$  and  $V_2$ ) across both PV modules, the value of effective impedance  $Z_{EFF}$  should be minimum. However, practically it is unavoidable to have zero value of  $Z_{EFF}$  but since the value of  $Z_{EFF}$  is frequency dependent. Therefore, it is possible to achieve the minimum value by operating the converter at frequencies near to the resonant frequency.

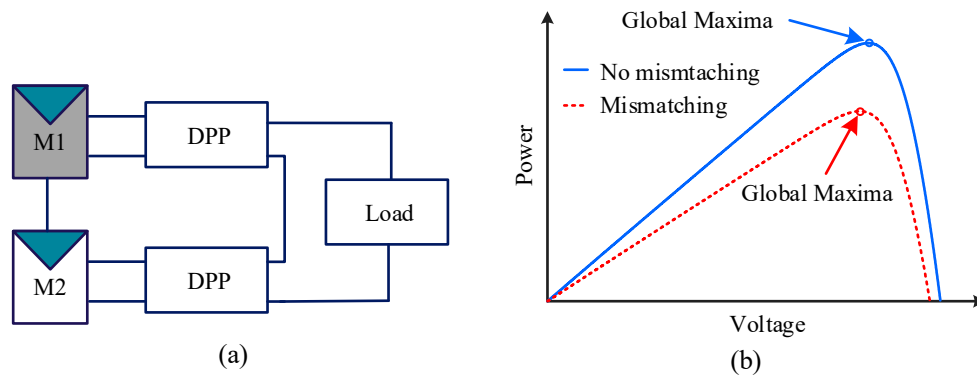


**Figure 2.** PV modules (M1 and M2) with parallel-connected DPP topologies: (a) schematic diagram when M1 is shaded and (b) P–V characteristic of series-connected two PV modules during mismatching and no mismatching.

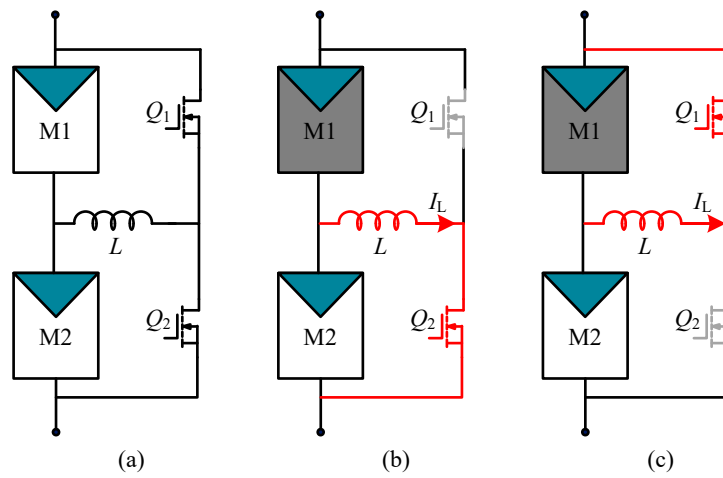


**Figure 3.** Switched-inductor (SL)-based PV–PV voltage balance converter [20]: (a) schematic diagram containing two series-connected PV modules M1 and M2 without shading; (b) M1 is shaded, where  $Q_1$  is ON and  $Q_2$  is OFF; and (c) M1 is shaded and  $Q_1$  is OFF and  $Q_2$  is ON. Here,  $I_L$  is a current passing through an inductor  $L$ .

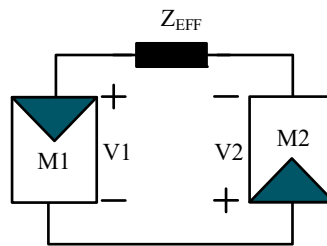


**Figure 4.** Equivalent circuit for the SL-based DPP technique. Here,  $Z_{EFF}$  is the effective impedance,  $V_1$ , and  $V_2$  are the voltages across the PV module M1 and M2, respectively.

Moreover, another important factor to consider in the design of the SL-based topology is the quality factor  $Q$ , which is given by expression (2)

$$Q = (1/R_{ESR}) \sqrt{L/C} \quad (2)$$

where  $L$  is the inductance shown in Figure 3 and  $C$  is the stray capacitance, which can be neglected as its value is very small. For practical reasons and to have adequate voltage stress across inductor  $L$ , the value of  $Q$  is selected in the range of 1–10 and the switching frequency is selected as 50 kHz.

The value of switching frequency is selected closer to the resonant frequency in order to have a minimum value of  $Z_{EFF}$ . For better understanding,  $Z_{EFF}$  can be considered as a series LC network whose impedance versus frequency curve is shown in Figure 5, which can be calculated by using (3). At lower frequencies (below resonant frequency), the topology behaves as overall capacitive. However, as the frequency increases, the value of  $Z_{EFF}$  decreases to its minimum value at the resonant frequency where the impedances of  $L$  and  $C$  cancels each other. Similarly, beyond the resonant frequency and at higher frequencies, the nature of  $Z_{EFF}$  is overall inductive. Therefore, the value of switching frequency is selected in the vicinity of resonant frequency to achieve a minimum value of  $Z_{EFF}$ , which will, in turn, equalizes the voltages of PV modules in a system. Moreover, the value of switching frequency is selected to be higher than the resonant frequency to achieve soft-switching operation for all the switches, which can minimize the switching power loss.

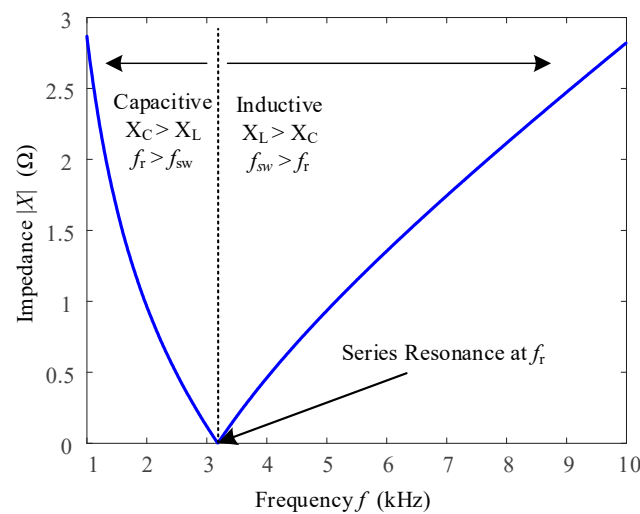


**Figure 5.** A curve showing the variation of impedance with frequency for a series resonant circuit.

$$|X| = |X_L| - |X_C| \quad (3)$$

where  $X_L$  is the inductive impedance and  $X_C$  is the capacitive impedance.

The power losses during partial shading are dependent upon the patterns of shading. Various schemes have been presented in the literature to minimize the detrimental effects caused by non-uniform shading [26]. One possibility is to reconfigure the interconnection PV modules in case if there is partial shading. The most commonly used interconnection scheme for PV arrays is series-parallel (SP). Configurations like the bridge-linked (BL), central-cross-tied (CCT), and total-cross-tied (TCT) (see Figure 6) can also be adopted to minimize the mismatching effect due to partial shading [27]. Although, it has been revealed that the TCT configuration yields maximum power for conventional bypass technique [28], more attempts have been made to mitigate the effects of partial shading using SP configurations due to its simplicity [29]. Using TCT enhances the longevity of the PV module with an estimated increase in a lifetime by 30% [30]. Alternately an electronic array reconfiguration scheme abbreviated as EAR has been proposed, which may modify the interconnection pattern of modules using electronic switches. In EAR, during operation and the decision of reconfiguration is based upon the pattern of shading, while control is achieved using a switch matrix [31]. The electrical reconfiguration using switches and relays, which can be effectively realized for small systems. However, for large PV arrays in solar parks, etc., the electronic switches, their interaction, and controllability becomes complex and difficult to handle due to the constraints of switching [32]. Similarly, another technique termed as disperse interconnection scheme (SDS) for multiple PV modules in an array has been presented in [33]. This technique is also based on changing the electrical configuration of the modules in the PV array. This technique has superior output yield in comparison to other

interconnection schemes as discussed in [29]. However, cost and complexity associated with the changing connections in large PV arrays can be cumbersome, and the overall system yield may become infeasible [29]. Therefore, various aspects by including efficiency and cost must be carefully considered for the optimal system design. A static reconfiguration is considered effective over other dynamic interconnection techniques [23]. The static reconfiguration technique does not involve the dynamic change of interconnection. It is based upon the one-time constant arrangement of PV modules with predefined interconnection settings in an array under different partial shading conditions [34,35]. Different interconnection topologies, which are discussed above—namely, SP, BL, and TCT for PV arrays—have been proposed. These interconnection schemes are tested by using intelligent power electronics to minimize power losses due to mismatch. The power electronic-based technique replaces the shunting bypass diodes, which are generally connected in parallel to PV modules in the array.

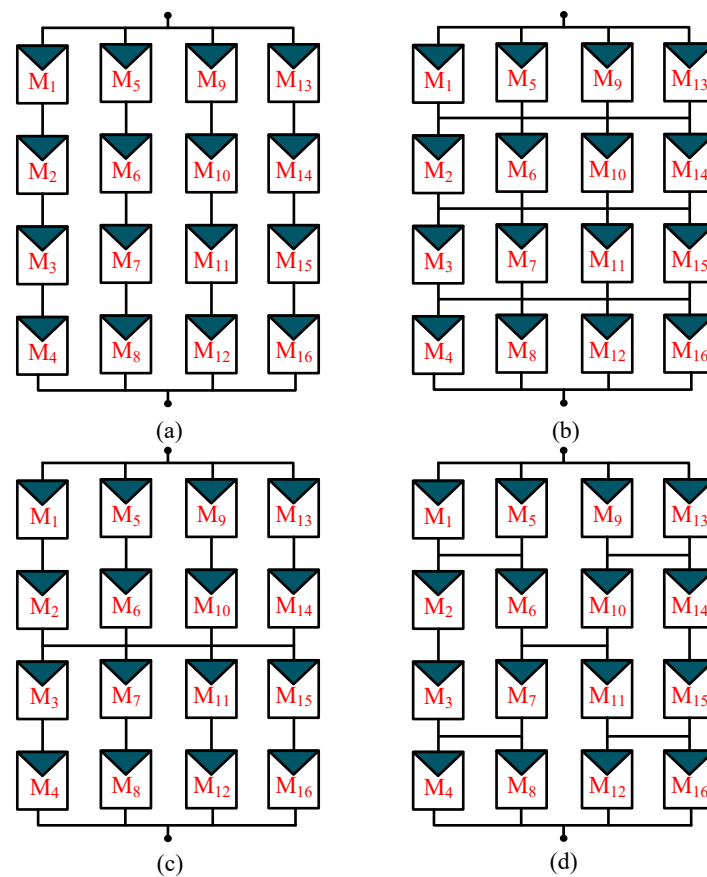


**Figure 6.** PV array topologies: (a) series-parallel (SP), (b) total-cross-tied (TCT), (c) central-cross-tied (CCT), and (d) bridge-linked (BL).

The performance analysis of above-mentioned interconnection schemes has been widely discussed with traditional bypass diodes in the literature so far. However, when DPP converters have adopted the performance of those configurations has not yet been explored. Therefore, in this paper, the four array interconnection schemes—i.e., the SP, TCT, CCT, and BL configurations with SL-DPP—are tested under different patterns of shading and irradiance. The performance of proposed schemes (SL-based interconnection schemes) is evaluated by introducing different shading patterns and its comparison with state of the art topology, i.e., bypass diode (for comparative analysis). This study uses a  $4 \times 4$  PV array of system, which has a size of 968 W. The output power and mismatch losses under various shading patterns with SL-DPP and bypass diodes are presented. The organization of the rest of the paper is given below. Section 2 introduces the different interconnection configurations and shading

pattern designs. Section 3 outlines various important results and based upon the highlighted results conclusions are outlined in Section 4.

## 2. Configurations and Shading Pattern Designs

The four interconnection schemes—i.e., the SP, TCT, CCT, and BL configurations—are compared at different shading patterns for the  $4 \times 4$  PV array. The PV array with these configurations using DPP converters and bypass diodes are evaluated. The rating of PV modules is given in Table 1. The rated maximum output power from the  $4 \times 4$  PV system is 968 Watt at  $1000 \text{ W/m}^2$  and STP. Different types of shading patterns including, one module shading, short wide, long narrow shading, central shading, and diagonal shading are applied at all above discussed interconnection schemes on  $4 \times 4$  PV array at different irradiances, as shown in Figure 7. The variations in irradiance from  $200 \text{ W/m}^2$  to  $800 \text{ W/m}^2$  with a difference of  $100 \text{ W/m}^2$  is considered to compare the performance of SL-based DPPs with conventional parallel-connected bypass diodes. Various shading pattern designs for PV array configuration schemes are as follows.

**Table 1.** Specification of the PV module at STC ( $1000 \text{ W/m}^2$  and  $25^\circ\text{C}$ ).

Parameters	Rating
Rated Peak Power ( $P_{\max}$ )	60 W
Voltage at MPP ( $V_{\text{mp}}$ )	17.10 V
Current at MPP ( $I_{\text{mp}}$ )	3.50 A
Open Circuit Voltage ( $V_{\text{oc}}$ )	21.10 V
Short Circuit Current ( $I_{\text{sc}}$ )	3.80 A

### 2.1. One Module Shading

In the condition of one module shading, one module from first row and first column is shaded from  $4 \times 4$  PV array, i.e., PV module M1, as shown in Figure 7a.

### 2.2. Short Wide Shading

For short wide shading, four PV modules from the first two rows and columns are shaded, i.e., M1, M2, M5, and M6, as shown in Figure 7b.

### 2.3. Long Narrow Shading

In long narrow shading, PV modules placed at the last column of PV array, which includes PV modules, M13, M14, M15, and M16 along with the last row, which are M4, M8, and M12 are not shaded, as shown in Figure 7c. Rest of all PV modules are shaded from  $4 \times 4$  PV array.

### 2.4. Central Shading

Four PV modules from the center are shaded—i.e., M6, M7, M10, and M11—while all other remain unshaded, as shown in Figure 7d.

### 2.5. Diagonal Shading

For diagonal shading M4, M7, M10, and M13 are shaded, as shown in Figure 7e. In diagonal shading, one module gets shaded from each row and column of a  $4 \times 4$  PV array for all configuration schemes.



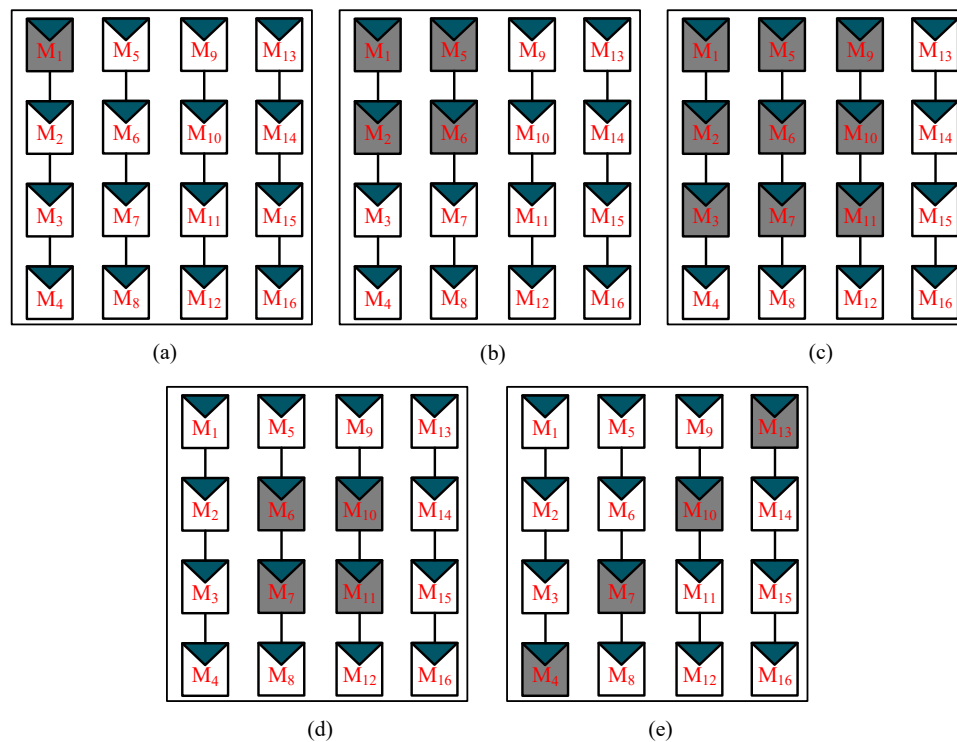


**Figure 7.** Shading pattern designs for PV array configuration schemes: (a) one module, (b) short wide, (c) long narrow, (d) central, and (e) diagonal.

### 3. Results and Discussion

The simulation results for the configurations with traditional bypass diodes and power electronic-based DPP architectures are shown in Figures 8–11. The systems are evaluated at 1000 W/m<sup>2</sup>, 800 W/m<sup>2</sup>, 600 W/m<sup>2</sup>, 500 W/m<sup>2</sup>, 400 W/m<sup>2</sup>, and 200 W/m<sup>2</sup> by using a power sim (PSIM).

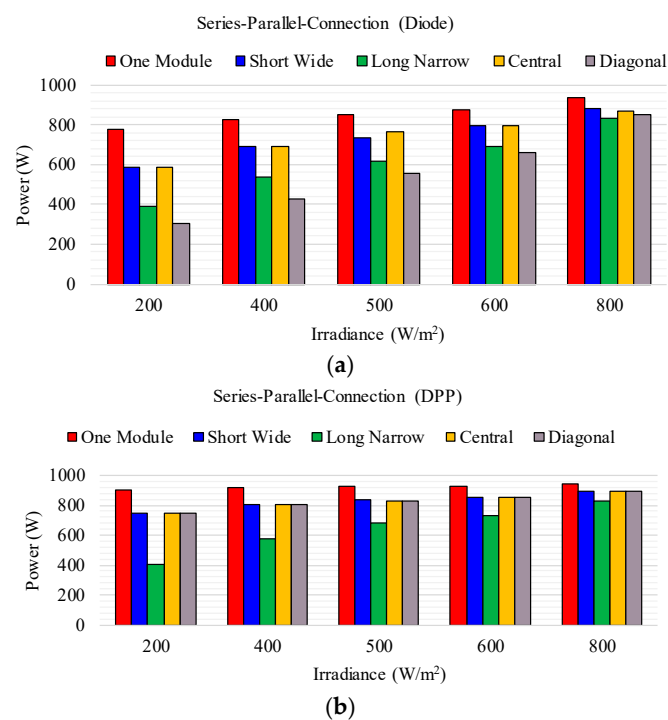


**Figure 8.** Output for series-parallel (SP) connection under various shading conditions with: (a) diode connection and (b) DPP connection.

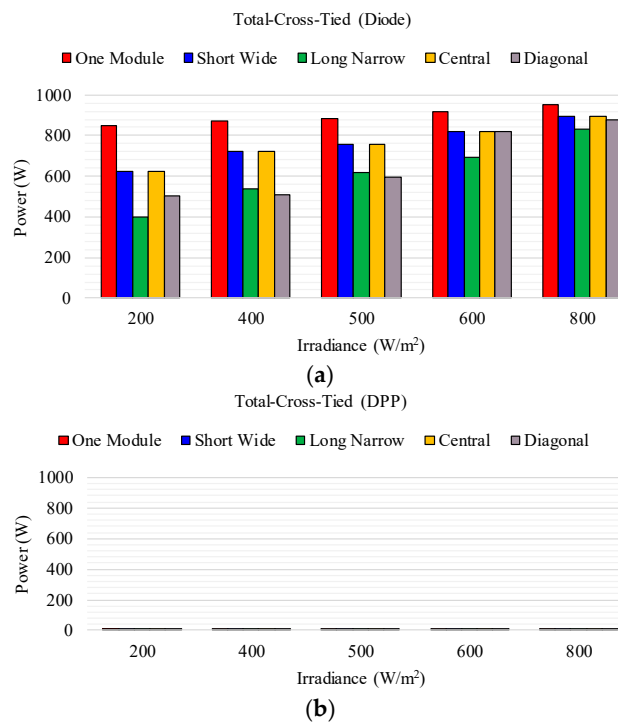


**Figure 9.** Output for total-cross-tied (TCT) connection under various shading conditions with: (a) diode connection and (b) DPP connection (zero output).

The unshaded modules in Figure 7 experience an irradiance of  $1000 \text{ W/m}^2$ . It is seen in Figures 8 and 10 that PV strings with DPP architectures have higher output power for the SP and CCT configurations than the systems with traditional bypass diodes. However, when DPP converters are adopted, there is almost zero or below  $1 \text{ W}$  of output power for all the shading scenarios with the TCT and BL configurations, as shown in Figures 9b and 11b. As the SL-based DPP architecture requires at least two series-connected PV modules for the converter to work properly, as shown in Figure 3. However, in TCT and BL architectures, their interconnections with other parallel PV strings affect the working principle of the used SL-based DPP topology.

In SP configuration, the output power for bypass diode and DPP under all shading patterns is shown in Figure 8a,b. The output power is  $778 \text{ W}$ ,  $826 \text{ W}$ ,  $847 \text{ W}$ ,  $872 \text{ W}$ , and  $933 \text{ W}$  with bypass diode for one module, short wide, long narrow, central, and diagonal shading patterns, respectively, as shown in Figure 8a. In SP, output power with proposed SL-based DPP architecture is  $905 \text{ W}$ ,  $918 \text{ W}$ ,  $924 \text{ W}$ ,  $930 \text{ W}$ , and  $942 \text{ W}$  at  $200 \text{ W/m}^2$ ,  $400 \text{ W/m}^2$ ,  $500 \text{ W/m}^2$ ,  $600 \text{ W/m}^2$ , and  $800 \text{ W/m}^2$ , respectively during one module, short wide, long narrow, central, and diagonal shading, respectively (see Figure 8b). For bypass diode technique, the power output in SP using short wide and central shading is almost similar as four PV modules are shaded under both schemes, two from each PV strings. Whereas, in the diagonal shading, each module is shaded from each parallel-connected PV string. Therefore, it has a more severe effect on output power, especially for diode bypass architecture, which can be seen from Figure 8a. DPP with SP interconnection, which is shown in Figure 8b has almost the same output power under given irradiances.

The power output received from CCT interconnection is shown in Figure 10. Similar to SP, in CCT one module shading has maximum power for all shading patterns, i.e.,  $821 \text{ W}$ ,  $857 \text{ W}$ ,  $870 \text{ W}$ ,  $900 \text{ W}$ , and  $945 \text{ W}$  at  $200 \text{ W/m}^2$ ,  $400 \text{ W/m}^2$ ,  $500 \text{ W/m}^2$ ,  $600 \text{ W/m}^2$ , and  $800 \text{ W/m}^2$ , respectively with bypass diode architecture. Similarly,  $905 \text{ W}$ ,  $918 \text{ W}$ ,  $925 \text{ W}$ ,  $930 \text{ W}$ , and  $942 \text{ W}$  for SL-based DPP architecture at  $200 \text{ W/m}^2$ ,  $400 \text{ W/m}^2$ ,  $500 \text{ W/m}^2$ ,  $600 \text{ W/m}^2$ , and  $800 \text{ W/m}^2$ , respectively under one module shading scheme.

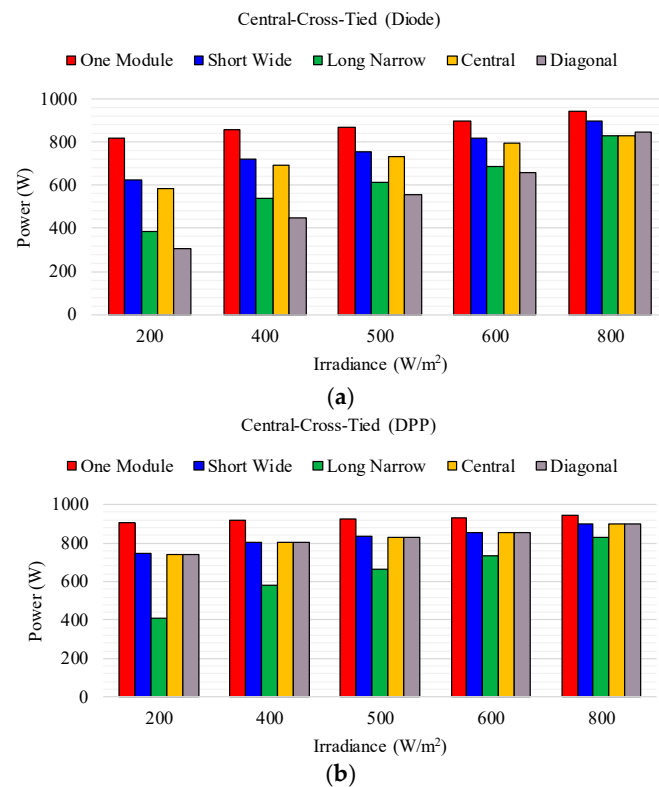


**Figure 10.** Output for central-cross-tied (CCT) connection under various shading conditions with: (a) diode connection and (b) DPP connection.

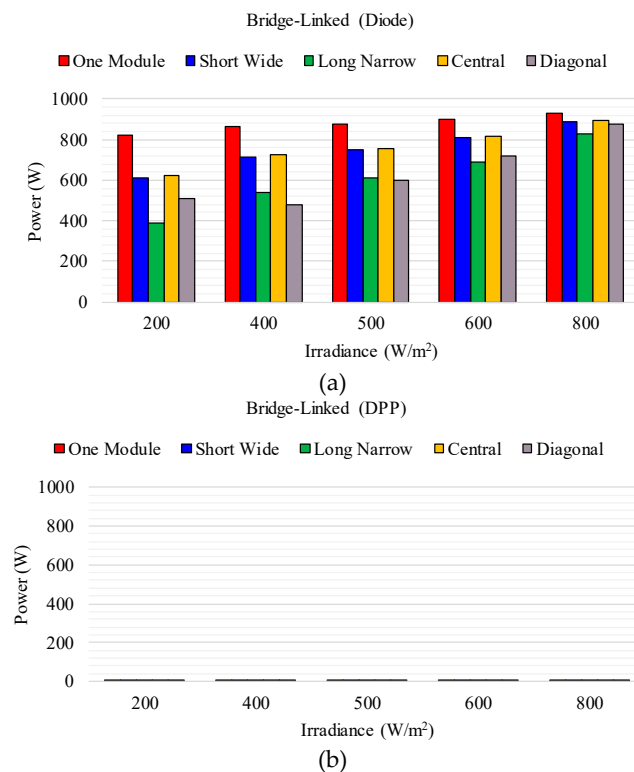


**Figure 11.** Output for bridge-linked (BL) connection under various shading conditions with: (a) diode connection and (b) DPP connection (zero output).

For short wide, long narrow, central, and diagonal shading the output power is given in Figure 10a,b with bypass diode and DPP, respectively. Figures 9 and 11 show the output power from TCT and

BL interconnections for the traditional diode. In TCT and BL connections, DPP architecture is not applicable as discussed before. Therefore, the output power is almost 0 W, as shown in Figures 9b and 11b. Power losses are also calculated from Figures 8 and 10 during one module, short wide, long narrow, central, and diagonal shading for SP and CCT traditional bypass diodes and DPP converters. These losses are calculated only for the SP and CCT interconnections because TCT and BL interconnection schemes are not applicable on the SL-based DPP converter. For instance, power losses during one module shading for the worst case—i.e., 200 W/m<sup>2</sup> are 15.34%, 10.66% for SP and CCT, respectively by using the bypass diode. It is only 1.52% for the DPP architecture by using SP and CCT interconnections during one module shading. The power losses decrease with an increase in irradiance. For short wide and long narrow shading at 200 W/m<sup>2</sup>, the power losses for traditional bypass diode are 24.19% and 19.12% during short wide and 40.42% and 40.73% during long narrow shading for SP and CCT, respectively. Similarly, at 200 W/m<sup>2</sup>, DPP architecture has 3.66% and 3.40% power losses during short wide shading for SP and CCT, respectively. Power loss for DPP during long wide shading is 37.51% and 40.58% for SP and CCT at 200 W/m<sup>2</sup>. For the rest of the irradiances, the power loss decreases as the irradiance increases both for diode and DPP.

The power losses for SP and CCT string interconnections during central and diagonal shading for diode at 200 W/m<sup>2</sup> is 24.19% both for SP and CCT while 4.11% by using DPP. During diagonal shading, it has similar power losses for SP and CCT interconnections, which is 60.85% for bypass diode and 4.05% for DPP at 200 W/m<sup>2</sup>. Similarly, these power losses decrease with an increase of irradiance in a diagonal shading pattern also. Overall, PV strings with SP and CCT interconnections with DPP architecture have more output power than a traditional diode. For short wide, central, and diagonal shading, PV strings with DPP architecture are producing almost the same output power because four PV modules are shaded for all of them. DPP architecture is not applicable to TCT and BL interconnections. In all, DPP extracts more power from the 4 × 4 PV array system than traditional bypass diode for all interconnection schemes where it is applicable. However, SL-based DPP topology has higher cost with a complex circuitry in comparison to traditional bypass diode topology.

#### 4. Conclusions

In this paper, a DPP converter has been used in PV modules with different static interconnection schemes including series-parallel (SP), total-cross-tied (TCT), central-cross-tied (CCT), and bridge-linked (BL). The power production from the PV modules under various interconnection schemes and mismatch conditions have been explored. More importantly, a comparison of the power production between the traditional bypass diode and the DPP-based architecture for a 4 × 4 PV array has been performed. It has been found that the two configurations—i.e., SP and CCT with the DPP converters—produce more power than traditional bypass diode-based architecture. On the other hand, TCT and BL configurations are not suitable for integrating the DPP converters due to their inherent hardware limitations. Hence, the DPP-based interconnection might be a promising solution to enhance the energy yield for PV modules with minimal mismatch power losses during partial shading conditions. It is especially suitable for the SP configuration, which is the most commonly used configuration in practice. However, the integration of DPP converters will inevitably increase the cost and complexity of the overall system, which requires further analysis.

**Author Contributions:** K.A.K.N., conceptualization, investigation, methodology, validation, writing—original draft preparation; Y.Y., project administration, supervision, writing—review and editing; M.N., writing—review and editing; D.S., supervision, writing—review and editing.

**Funding:** This research received no external funding.

**Conflicts of Interest:** The authors declare no conflict of interest.

## References

1. Cancino-Solórzano, Y.; Paredes-Sánchez, J.P.; Gutiérrez-Trashorras, A.J.; Xiberta-Bernat, J. The development of renewable energy resources in the State of Veracruz, Mexico. *Utilities Policy* **2016**, *39*, 1–4. [\[CrossRef\]](#)
2. Fahrenbruch, A.; Bube, R. *Fundamentals Of Solar Cells: Photovoltaic Solar Energy Conversion*; Elsevier: Amsterdam, The Netherlands, 2012; ISBN 978-0-32-314538-1.
3. Subudhi, B.; Pradhan, R. A Comparative Study on Maximum Power Point Tracking Techniques for Photovoltaic Power Systems. *IEEE Trans. Sustain. Energy* **2013**, *4*, 89–98. [\[CrossRef\]](#)
4. Sahoo, S.K. Renewable and sustainable energy reviews solar photovoltaic energy progress in India: A review. *Renew. Sustain. Energy Rev.* **2016**, *59*, 927–939. [\[CrossRef\]](#)
5. Ahmed, J.; Salam, Z. A critical evaluation on maximum power point tracking methods for partial shading in PV systems. *Renew. Sustain. Energy Rev.* **2015**, *47*, 933–953. [\[CrossRef\]](#)
6. Niazi, K.A.K.; Yang, Y.; Khan, H.A.; Sera, D. Performance Benchmark of Bypassing Techniques for Photovoltaic Modules. In Proceedings of the 2019 IEEE Applied Power Electronics Conference and Exposition (APEC), Anaheim, CA, USA, 17–21 March 2019.
7. Pareek, S.; Dahiya, R. Enhanced power generation of partial shaded photovoltaic fields by forecasting the interconnection of modules. *Energy* **2016**, *95*, 561–572. [\[CrossRef\]](#)
8. Niazi, K.; Khan, H.A.; Amir, F. Hot-spot reduction and shade loss minimization in crystalline-silicon solar panels. *J. Renew. Sustain. Energy* **2018**, *10*, 1–8. [\[CrossRef\]](#)
9. Yang, Y.; Kim, K.A.; Blaabjerg, F.; Sangwongwanich, A. *Advances in Grid-Connected Photovoltaic Power Conversion Systems*; Woodhead Publishing: Cambridge, UK, 2018; ISBN 978-0-08-102342.
10. Ahsan, S.; Niazi, K.A.K.; Khan, H.A.; Yang, Y. Hotspots and performance evaluation of crystalline-silicon and thin-film photovoltaic modules. *Microelectron. Reliab.* **2018**, *88–90*, 1014–1018. [\[CrossRef\]](#)
11. Ishaque, K.; Salam, Z. A review of maximum power point tracking techniques of PV system for uniform insolation and partial shading condition. *Renew. Sustain. Energy Rev.* **2013**, *19*, 475–488. [\[CrossRef\]](#)
12. Eltawil, M.A.; Zhao, Z. MPPT techniques for photovoltaic applications. *Renew. Sustain. Energy Rev.* **2013**, *25*, 793–813. [\[CrossRef\]](#)
13. Nasir, M.; Zia, M.F. Global maximum power point tracking algorithm for photovoltaic systems under partial shading conditions. In Proceedings of the 16th International Power Electronics and Motion Control Conference and Exposition, Antalya, Turkey, 21–24 September 2014.
14. Alajmi, B.N.; Ahmed, K.H.; Finney, S.J.; Williams, B.W. A Maximum Power Point Tracking Technique for Partially Shaded Photovoltaic Systems in Microgrids. *IEEE Trans. Ind. Electron.* **2013**, *60*, 1596–1606. [\[CrossRef\]](#)
15. Niazi, K.; Akhtar, W.; Khan, H.A.; Sohaib, S.; Nasir, A.K. Binary Classification of Defective Solar PV Modules Using Thermography. In Proceedings of the 2018 IEEE 7th World Conference on Photovoltaic Energy Conversion (WCPEC), Waikoloa, HI, USA, 10–15 June 2018.
16. Liu, Y.-H.; Liu, C.-L.; Huang, J.-W.; Chen, J.-H. Neural-network-based maximum power point tracking methods for photovoltaic systems operating under fast changing environments. *Sol. Energy* **2013**, *89*, 42–53. [\[CrossRef\]](#)
17. Daraban, S.; Petreus, D.; Morel, C. A novel MPPT (maximum power point tracking) algorithm based on a modified genetic algorithm specialized on tracking the global maximum power point in photovoltaic systems affected by partial shading. *Energy* **2014**, *74*, 374–388. [\[CrossRef\]](#)
18. Salam, Z.; Ahmed, J.; Merugu, B.S. The application of soft computing methods for MPPT of PV system: A technological and status review. *Appl. Energy* **2013**, *107*, 135–148. [\[CrossRef\]](#)
19. Niazi, K.A.K.; Yang, Y.; Sera, D. Review of mismatch mitigation techniques for PV modules. *IET Renew. Power Gener.* **2019**. [\[CrossRef\]](#)
20. Kim, K.A.; Shenoy, P.S.; Krein, P.T. Converter Rating Analysis for Photovoltaic Differential Power Processing Systems. *IEEE Trans. Power Electron.* **2015**, *30*, 1987–1997. [\[CrossRef\]](#)
21. Jeon, Y.; Lee, H.; Kim, K.A.; Park, J. Least Power Point Tracking Method for Photovoltaic Differential Power Processing Systems. *IEEE Trans. Power Electron.* **2017**, *32*, 1941–1951. [\[CrossRef\]](#)
22. Khan, O.; Xiao, W. Review and qualitative analysis of submodule-level distributed power electronic solutions in PV power systems. *Renew. Sustain. Energy Rev.* **2017**, *76*, 516–528. [\[CrossRef\]](#)

23. Stauth, J.T.; Seeman, M.D.; Kesarwani, K. Resonant Switched-Capacitor Converters for Sub-module Distributed Photovoltaic Power Management. *IEEE Trans. Power Electron.* **2013**, *28*, 1189–1198. [[CrossRef](#)]
24. Tahmasbi-Fard, M.; Tarafdar-Hagh, M.; Pourpayam, S.; Haghray, A. A Voltage Equalizer Circuit to Reduce Partial Shading Effect in Photovoltaic String. *IEEE J. Photovolt.* **2018**, *8*, 1102–1109. [[CrossRef](#)]
25. Jeong, H.; Lee, H.; Liu, Y.; Kim, K.A. Review of Differential Power Processing Converter Techniques for Photovoltaic Applications. *IEEE Trans. Energy Convers.* **2019**, *34*, 351–360. [[CrossRef](#)]
26. Karatepe, E.; Boztepe, M.; Çolak, M. Development of a suitable model for characterizing photovoltaic arrays with shaded solar cells. *Sol. Energy* **2007**, *81*, 977–992. [[CrossRef](#)]
27. La Manna, D.; Li Vigni, V.; Riva Sanseverino, E.; Di Dio, V.; Romano, P. Reconfigurable electrical interconnection strategies for photovoltaic arrays: A review. *Renew. Sustain. Energy Rev.* **2014**, *33*, 412–426. [[CrossRef](#)]
28. Satpathy, P.R.; Jena, S.; Sharma, R. Power enhancement from partially shaded modules of solar PV arrays through various interconnections among modules. *Energy* **2018**, *144*, 839–850. [[CrossRef](#)]
29. Kadri, R.; Andrei, H.; Gaubert, J.-P.; Ivanovici, T.; Champenois, G.; Andrei, P. Modeling of the photovoltaic cell circuit parameters for optimum connection model and real-time emulator with partial shadow conditions. *Energy* **2012**, *42*, 57–67. [[CrossRef](#)]
30. Satpathy, P.R.; Jena, S.; Jena, B.; Sharma, R. Comparative study of interconnection schemes of modules in solar PV array network. In Proceedings of the 2017 International Conference on Circuit, Power and Computing Technologies (ICCPCT), Kollam, India, 20–21 April 2017.
31. Velasco-Quesada, G.; Guinjoan-Gispert, F.; Pique-Lopez, R.; Roman-Lumbreras, M.; Conesa-Roca, A. Electrical PV Array Reconfiguration Strategy for Energy Extraction Improvement in Grid-Connected PV Systems. *IEEE Trans. Ind. Electron.* **2009**, *56*, 4319–4331. [[CrossRef](#)]
32. Lavado Villa, L.F.; Ho, T.-P.; Crebier, J.-C.; Raison, B. A Power Electronics Equalizer Application for Partially Shaded Photovoltaic Modules. *IEEE Trans. Ind. Electron.* **2013**, *60*, 1179–1190. [[CrossRef](#)]
33. Satpathy, P.R.; Sharma, R.; Jena, S. A shade dispersion interconnection scheme for partially shaded modules in a solar PV array network. *Energy* **2017**, *139*, 350–365. [[CrossRef](#)]
34. Malathy, S.; Ramaprabha, R. Reconfiguration strategies to extract maximum power from photovoltaic array under partially shaded conditions. *Renew. Sustain. Energy Rev.* **2018**, *81*, 2922–2934. [[CrossRef](#)]
35. Rana, A.S.; Nasir, M.; Khan, H.A. String level optimisation on grid-tied solar PV systems to reduce partial shading loss. *IET Renew. Power Gener.* **2017**, *12*, 143–148. [[CrossRef](#)]



© 2019 by the authors. Licensee MDPI, Basel, Switzerland. This article is an open access article distributed under the terms and conditions of the Creative Commons Attribution (CC BY) license (<http://creativecommons.org/licenses/by/4.0/>).